Biological Channeling of a Reactive Intermediate in the Bifunctional Enzyme DmpFG

Natalie E. Smith, Alice Vrielink, Paul V. Attwood, and Ben Corry*
School of Chemistry and Biochemistry, The University of Western Australia, Perth, Western Australia

ABSTRACT It has been hypothesized that the bifunctional enzyme DmpFG channels its intermediate, acetaldehyde, from one active site to the next using a buried intermolecular channel identified in the crystal structure. This channel appears to switch between an open and a closed conformation depending on whether the coenzyme NAD^+ is present or absent. Here, we applied molecular dynamics and metadynamics to investigate channeling within DmpFG in both the presence and absence of NAD^+. We found that substrate channeling within this enzyme is energetically feasible in the presence of NAD^+ but was less likely in its absence. Tyr-291, a proposed control point at the channel's entry, does not appear to function as a molecular gate. Instead, it is thought to orientate the substrate 4-hydroxy-2-ketovalerate in DmpG before reaction occurs, and may function as a proton shuttle for the DmpG reaction. Three hydrophobic residues at the channel's exit appear to have an important role in controlling the entry of acetaldehyde into the DmpF active site.

INTRODUCTION

Biological systems rely on a complex array of metabolic pathways and multistep catalytic cycles to function successfully (1). Although traditionally it was assumed that the products of one enzyme would be released into the bulk media and enter the active site of the second enzyme via diffusion, a more obvious route for the transport of intermediates would involve direct transfer from one active site to the other, completely avoiding equilibration with the bulk solvent (2,3). This mechanism, involving the transport of intermediates directly from one active site to another, is known as substrate channeling.

This process is known to occur in a number of multifunctional enzymes via a buried molecular channel or an electrostatic highway on the surface of the enzyme (4,5). Substrate channeling via a buried molecular channel serves several purposes within a multienzyme process. First, it increases the rate of the reaction, avoiding unfavorable equilibria and allowing the intermediate to be transferred more rapidly than diffusion-mediated processes would allow (3). Second, it ensures that labile intermediates will not be degraded or participate in any reactions before entering the second active site. Finally, in certain cases, the channel also serves to protect the organism from toxic intermediates (6).

One enzyme for which substrate channeling has been proposed is 4-hydroxy-2-ketovalerate aldolase-aldehyde dehydrogenase (acylating) (DmpFG). DmpFG is a microbial, heteromeric enzyme comprised of two subunits, DmpG and DmpF (2), as shown in Fig. 1 *A*. DmpFG catalyzes the final two steps of the *meta*-cleavage pathway of catechol and its methylated substituents. Catechol, or 1,2-dihydroxybenzene, is an intermediate that is formed from the breakdown of toxic waste products such as naphthalene, salicylates, benzoates, and phenol (7,8).

DmpG, the aldolase, catalyzes the cleavage of the substrate 4-hydroxy-2-ketovalerate (HKV) to acetaldehyde (AALD) with the release of pyruvate (Fig. 1 *B*). AALD is the intermediate in this process and it must reach the active site of DmpF, the dehydrogenase. However, AALD is both labile and toxic to bacteria, and therefore its release into the bulk solvent would not be advantageous to the organism. An alternative route to the second active site has been proposed based on an examination of the crystal structure of DmpFG, which revealed a 29 Å water-filled channel linking the aldolase and dehydrogenase active sites (2). Although this channel appears to be an ideal conduit for transporting AALD from one active site to the other, it has not yet been shown that this is the actual route taken within the enzyme DmpFG.

Although kinetic evidence of channeling has not been obtained for DmpFG, extensive biochemical, kinetic, and site-directed mutagenesis studies have been carried out on the close ortholog, BphI-BphJ (where BphI and BphJ have 56% and 55% sequence similarity with DmpG and DmpF, respectively) (9–12). BphI-BphJ are two enzymes in the polychlorinated biphenyls degradation pathway of *Burkholderia xenovorans* LB400, and similarly to DmpFG, they catalyze the conversion of 4-hydroxy-2-ketoacids to a coenzyme A derivative and pyruvate. Again, a toxic aldehyde intermediate needs to move between the two spatially distinct active sites. These studies showed conclusively that the aldehyde intermediate is channeled from the BphI active site to that of BphJ within the enzyme complex (9,11). To date, no structure has been obtained for BphI-BphJ. In this study, we combined the structural information

Submitted September 12, 2011, and accepted for publication January 3, 2012.

*Correspondence: ben.corry@anu.edu.au

Ben Corry's present address is Research School of Biology, The Australian National University, Canberra, Australian Capital Territory, Australia.

Editor: Patrick Loria.

0006-3495/12/02/0868/10 $2.00

doi: 10.1016/j.bpj.2012.01.029

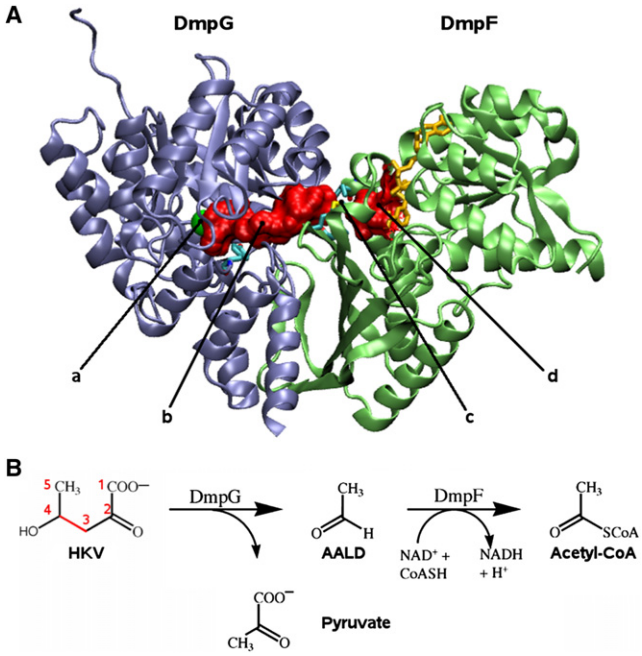

FIGURE 1 (*A*) DmpFG heterodimer, showing the DmpG (*left*) and DmpF (*right*) subunits. (*a*) The position of the DmpG active site (aldolase) with the central Mn^{2+} ion. (*b*) The solvent-accessible surface of a water-filled intramolecular channel reaching from the aldolase to the dehydrogenase active site (*red*). (*c*) The HT at the channel's exit. (*d*) The position of the DmpF active site (dehydrogenase). (*B*) The overall reaction catalyzed by DmpFG. The toxic intermediate AALD that forms in the aldolase active site is thought to be transported down an intramolecular channel to the dehydrogenase active site in DmpF (2). The HKV carbons are numbered from 1 to 5.

obtained by Manjasetty et al. (2) from DmpFG with the biochemical observations of BphI-BphJ to form a more comprehensive picture of this unique class of bifunctional enzymes and establish the mechanism by which they function as dynamic entities.

The mode of transport of the intermediate through the channel is a topic of considerable interest because so little is known about the process. Many of the active sites linked in this way are allosterically coupled, which means that the activity of the active sites is synchronized (3). Of interest, in DmpFG the activity of the aldolase (DmpG) appears to be allosterically modulated by the binding of the coenzyme NAD^+ to DmpF (13). This implies that there is a close working relationship between these two enzymes. If channeling occurs between the aldolase and dehydrogenase active sites, synchronization of their catalytic activities would be necessary to prevent the buildup of intermediate in the channel. In this context, a number of questions relating to DmpFG and substrate channeling in general arise: Is this coupled behavior common to all enzymes that have channeling activity? On the same note, how do these active sites synchronize their activity? Do changes in conformation occur before or during the channeling event? Is this process directional, and if so, what prevents the intermediate from back-tracking in the channel? Finally, what prevents the intermediate from escaping the channel?

An examination of the DmpFG crystal structure revealed two constricted regions that were assumed to be control points at the entry and exit of the channel. The first of these was Tyr-291 at the entry to the channel in the DmpG active site. Its position in the crystal structure was denoted as closed because it appeared to seal off the entry to the channel. A second position was modeled for this residue, suggesting a possible open conformation (2). The second proposed control point was composed of three residues at the channel's exit in the DmpF active site: Ile-172, Ile-196, and Met-198. Collectively, these residues are known as the hydrophobic triad (HT). These side chains were seen to adopt multiple conformations that varied depending on the state of NAD^+ binding to the protein. It was noted that in the apo-enzyme form of DmpFG, in the absence of NAD^+, all conformations of the HT closed the channel. In contrast, when DmpFG was in the holo-enzyme form with NAD^+ bound, the residues changed position such that the channel was now more open. In this study, we sought to determine whether Tyr-291 and the HT are control points for the entry and exit of AALD in the channel, and if so, how this takes place.

Although methods such as high-resolution x-ray crystallography, site-directed mutagenesis, and transient-state techniques have provided some insight into the substrate channeling process (2,6,14–16), the mechanisms and dynamics involved in transferring the intermediates into and through the channel have not been extensively studied. Molecular dynamics (MD) simulations provide one way to observe such molecular motion over time, but although this approach has been widely applied to the study of permeation in transmembrane channels, there are very few examples of its application to substrate channeling in enzymes. Fan et al. (17) used free-energy MD to investigate the mode used by the enzyme carbamoyl phosphate synthetase to transport the products ammonia and ammonium through one of its two intermolecular channels. A related Brownian dynamics approach was used to study the transport of an intermediate on an external electrostatic highway (18). In this work, we employed both equilibrium MD and metadynamics to study the channeling of AALD in DmpFG and to ascertain the role of specific residues in controlling this process.

METHODS

DmpFG-substrate systems

For this study we used two DmpFG-substrate systems: holo-enzyme DmpFG with NAD^+ bound, and apo-enzyme DmpFG without NAD^+. The coordinates of both the holo and apo structures were obtained from the protein structure database, and the structure of DmpFG was obtained as a tetramer of DmpFG heterodimers (1NVM.pdb). Each protein was solvated in a 115 × 80 × 85 Å TIP3P water box with 300 mM NaCl and

simulated with periodic boundary conditions and the S isomer of HKV in the DmpG active site. Mn^{2+} and oxalate were present in the crystal structure, which allowed us to obtain the starting position of HKV by superimposing the appropriate region of HKV over the oxalate. Ordered waters from the crystal structure were included in the simulation systems. Constant temperature (310 K) and pressure (1 atm) were maintained and the particle mesh Ewald method was used to compute the complete electrostatics of the system with 2 fs time steps (19). The CHARMM27 force field (20) was used for the protein atoms and substrates, and the parameters for the central Mn^{2+}, deprotonated Tyr, enolate, and HKV were determined using both ab initio and MD techniques (21–24) with the programs Gaussian 03 (25) and NAMD (26).

Before collecting data, we performed a series of equilibration steps. The computed positions for all hydrogen atoms were energy-minimized for 5 ps while nonhydrogen atoms remained fixed. Water and ions were then minimized for 5 ps and subsequently equilibrated with 50 ps of MD simulation while the protein and substrates were kept fixed. This was followed by 20 ps of minimization. Harmonic restraints were applied to the protein atoms and gradually decreased over 250 ps from 20.0, 10.0, 5.0, and 2.5 to 0.5 kcal/mol/Å^2. This was followed by 250 ps of equilibration with no restraints on the protein. The final modeled position of HKV was used to position both enolate (the precursor of pyruvate) and AALD in the DmpG active site. AALD was fixed in position and the system was equilibrated for another 10 ps. The starting position of AALD used in all of these simulations, including the metadynamics, can be seen in Fig. S1 in the Supporting Material. We carried out the initial simulations on four permutations of Tyr-291 using the experimentally derived coordinates from the crystal structure of holo-enzyme DmpFG with NAD^+ bound. These included Tyr-291 beginning in the proposed open and closed positions in both a protonated and deprotonated state.

The next simulations used both apo and holo-enzyme DmpFG. Both systems were made with Cys-132 in both its protonated and deprotonated state, leading to a total of four systems:

DmpFG with protonated Cys-132 + NAD^+
DmpFG with deprotonated Cys-132 + NAD^+
DmpFG with protonated Cys-132
DmpFG with deprotonated Cys-132

After equilibration was completed, 200 ns of MD simulation were obtained for each of the four systems. All molecular graphics were generated using VMD (27).

Metadynamics

Because the channel within DmpFG is nonuniform in shape and is lined with bulky hydrophobic side chains that impede the motion of AALD, techniques such as umbrella sampling for the MD studies were inefficient. To circumvent this problem, we chose to apply metadynamics, which uses a history-based biasing potential to accelerate rare events, allowing processes that occur on a long timescale to be observed in a more practical timeframe (28,29). In this method, we apply the biasing potential to a collective variable that describes the event in question by summing a series of repulsive Gaussians that are deposited along the trajectory every τ_G steps as the simulation progresses. This increasing potential allows the system to escape from local free-energy minima and sample more of the free-energy landscape. Ultimately, the summed Gaussians can be used to reconstruct the free-energy surface of the system. In this case, the collective variable was chosen to be the dynamic projection (DistanceZ) of the center of mass of AALD onto the axis defined by Mn^{2+} in the DmpG active site and the α-carbon atom of Cys-132 in the DmpF active site. Thus, the collective variable defines the position of AALD in the channel with the origin at the midpoint of the channel (Fig. S1).

Both the apo and holo-enzyme systems with deprotonated Cys-132 were used for metadynamics simulations with a hill weight of 0.05 kcal/mol, a hill width of 0.3 Å, and a hill frequency of 200 fs. All other variables, including the initial position of AALD in the DmpG active site, were maintained the same as in the equilibrium MD simulations. Simulations were continued until the AALD exited the channel. Ten separate metadynamics simulations leading to 10 independent free-energy profiles were obtained for the system with NAD^+, and nine were obtained for the system without NAD^+. These were averaged to obtain a single free-energy profile for each system.

RESULTS AND DISCUSSION

Tyr-291 and movement of AALD into the channel

It has been hypothesized that Tyr-291 serves two functions in DmpG: 1), as a proton shuttle in the aldolase active site reaction; and 2), as a control point at the channel's entry. This implies that there should be two different protonation states for this residue as well as both an open and closed position that would allow or prevent AALD from entering the channel, respectively. To investigate this, we set up four different simulation systems, described as open-protonated (OP), open-deprotonated (OD), closed-protonated (CP), and closed-deprotonated (CD) based on the two positions of the side chain as discussed by Manjasetty et al. (2). We used 1.6 ns of equilibrium MD simulation to study the effect of each of these permutations on the behavior of Tyr-291. This was repeated in the presence of AALD.

For the systems without AALD, we found that there were two favored orientations of Tyr-291. This can be seen most clearly by plotting the distance between the hydroxyl oxygen of Tyr-291 and Mn^{2+} (Fig. 2 *A*). Further investigation revealed that the two tyrosine positions, at distances of ~5.5 Å and 4 Å from Mn^{2+}, were oriented toward the bound enolate and His-21, respectively. The Tyr-291 dihedral CA-CB-CG-CD1 shown in Fig. 2 *B* is a torsion about the plane of the Tyr-291 carbon ring. It is evident that when Tyr-291 is oriented toward His-21 (CD, OP, and OD), the plane of the Tyr-291 ring is not as free to rotate and is predominantly maintained at an angle of ~40°. In contrast, in the CP system this dihedral angle is free to adopt multiple orientations between 40° and 90° throughout the time course of the simulation. This is further depicted in Fig. S2, where *A* is the OD system, and *B* and *C* are two points in the CP system with dihedrals of 40° and 90°, respectively. These positions are in agreement with those shown in the proposed proton shuttling mechanism where the open position has Tyr-291 oriented toward His-21 and the closed position has Tyr-291 oriented toward enolate (2). In fact, the closed position from the crystal structure has a dihedral of 85.5° and is 5.6 Å away from the central Mn^{2+}, which is well within the range of values shown by the CP system.

The open position is maintained by a series of H-bonds either directly from the Tyr-291 hydroxyl oxygen to His-21 as in the CD system, or from the Tyr-291 hydroxyl oxygen to two waters as in the OP and OD systems (Fig. S2 *A*). Because one of these waters (water 403) is coordinated to

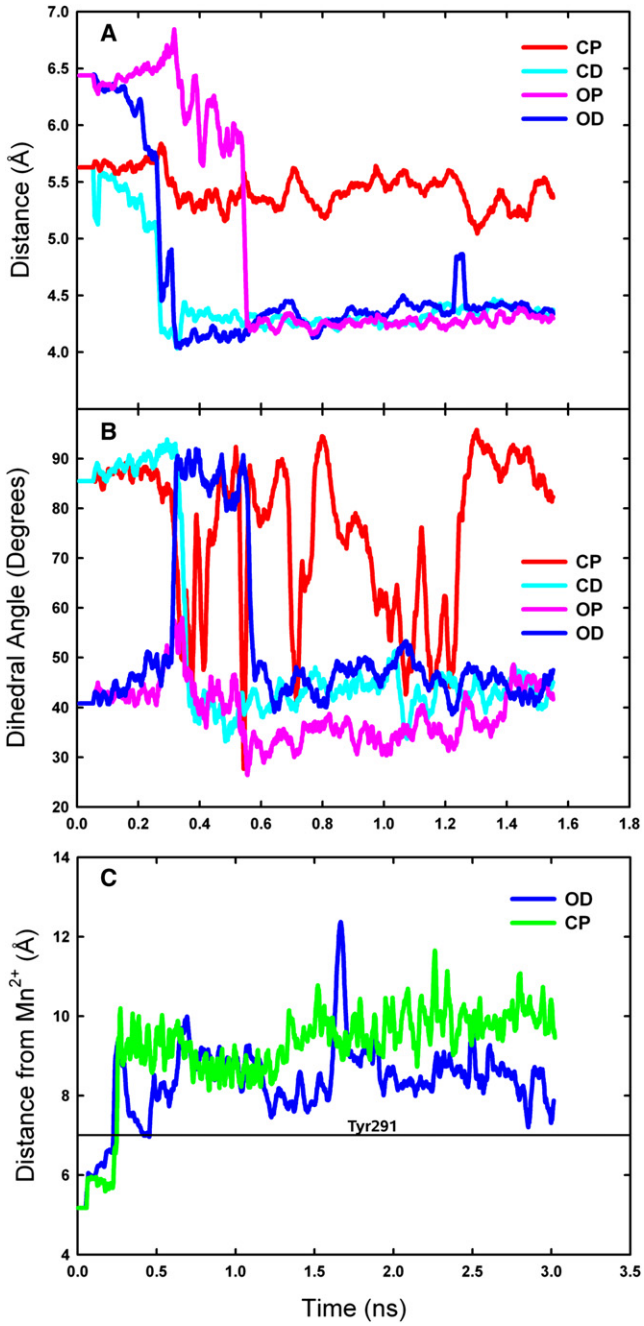

FIGURE 2 (*A*) Distance from the central Mn^{2+} to the Tyr-291 hydroxyl oxygen for the CP, CD, OP, and OD systems. (*B*) The Tyr-291 dihedral (CA-CB-CG-CD1) for the CP, CD, OP, and OD system. (*C*) The distance of AALD from the central Mn^{2+} for the OD and the CP systems.

the central Mn^{2+} and is not free to move, Tyr-291 is maintained in this orientation throughout the simulation. In contrast, the closed position seems to be predominantly maintained by a close and stable interaction between the Tyr-291 hydroxyl hydrogen and the methylene group of the enolate (Fig. S2, *B* and *C*). His-21 H-bonds with Arg-17 and a water molecule. At points in this simulation, this water H-bonds with both water 403 and Tyr-291, forming a close connection between Tyr-291, enolate, and His-21 as would be expected in the proposed reaction mechanism (2).

Having demonstrated the presence of two preferred positions for Tyr-291, we next examined whether these positions influence the entry of AALD into the channel. In this case, we analyzed only two systems, OD and CP, which correspond to the two most likely configurations obtained in our previous simulations as described above. The starting dihedral of the CP system was selected as ~90° because this was considered to be the most closed state, as shown in Fig. S2 *C*. We found that Tyr-291 adopted the same two positions with or without AALD present. We also found that regardless of both the position and protonation state of Tyr-291, AALD was able to pass Tyr-291 (located ~7 Å from Mn^{2+}) and enter the channel within 0.25 ns (Fig. 2 *C*). Therefore, the position of Tyr-291 does not control the passage of AALD into the channel when the intermediate enolate is present in the active site.

Although these results suggest that Tyr-291 could indeed function as a proton shuttle in the DmpG reaction, it was recently found in the close ortholog of DmpFG, BphI-BphJ, that when the equivalent of Tyr-291, Tyr-290, was mutated to serine or phenylalanine, the catalytic efficiency of the reaction decreased only threefold (12). This implies that although Tyr-291 appears to be involved in this reaction, it does not have a vital role as a proton shuttle (12). Another possibility is that another residue within the active site, or equilibration with water, can compensate for the loss of Tyr-290. Of interest, it was also noted in the Tyr290Phe mutant that the efficiency of channeling decreased by >30% relative to wild-type (WT) BphI-BphJ (11). The lack of a hydroxyl group on phenylalanine removes the ability of this residue to form H-bond interactions with the enolate or His-20, and allows the side chain to fluctuate freely, impeding the motion of AALD into the channel. This result provides indirect evidence of the importance of Tyr-291 in allowing the entry of AALD into the channel. It also raises questions concerning the channel closed state. Our MD results show that the channel is not closed in any of the positions proposed in the structural study of DmpFG. We also noted that the channel remained open in the simulations with HKV in the active site. Because all simulations were carried out starting with a ligand bound in the DmpG active site, it is possible that Tyr-291 enters a closed position in the absence of a bound ligand. Wang et al. (10) found that BphI follows an ordered sequential mechanism whereby the aldehyde product must leave the active site before pyruvate is released. In the context of Tyr-290 in BphI, and Tyr-291 in DmpG, this would maintain the tyrosine in a position that is favorable for entry of AALD into the channel.

The aldolase reaction in WT BphI-BphJ is stereoselective, with S-HKV being the preferred substrate (9,10). It was previously found that both the Tyr290Ser and Tyr290Phe mutants lose this stereoselectivity (12). To understand this more clearly, we obtained 2 ns of equilibrium MD simulation

for six simulation systems (WT DmpFG and the Tyr291Ser and Tyr291Phe mutants, each with S and R-HKV). In these simulations, both mutant systems allowed HKV to rotate freely about the C2-C3-C4-C5 dihedral (see Fig. 1 *B*), which allowed the substrate to significantly change its orientation in the active site.

These results for the mutants can be seen in Fig. 3, *C* and *D*, where S and R-HKV have both assumed a similar orientation in the active site of the Tyr291Ser mutant. In both cases, the HKV hydroxyl is oriented correctly for base attack by His-21, which supports the mechanisms proposed by both Manjasetty (2) and Baker et al. (12). This is in clear contrast to what was observed in WT DmpFG, as shown in Fig. 3, *A* and *B*. Although the position of S-HKV is maintained by a series of H-bonds to the Tyr-291 hydroxyl oxygen and water, R-HKV folds back on itself, forming a close and stable intramolecular interaction between its hydroxyl hydrogen and O2. Whereas the position of S-HKV is maintained by a series of hydrogen bonds to the Tyr-291 hydroxyl oxygen and water, R-HKV folds back on itself forming a close and stable intramolecular interaction between its hydroxyl hydrogen and O2. A steric clash between the Tyr-291 hydroxyl and HKV C5 methyl group prevents the R isomer from rotating in the active site, consistent with a previous finding by Baker et al. (12). Thus, the hydroxyl group remains oriented away from His-21, ultimately preventing a reaction from occurring in WT DmpG. However, because we currently lack biochemical data for the binding of R-HKV within DmpG, we must also consider the possibility that R-HKV cannot bind to the DmpG active site. This change in stereoselectivity suggests that the presence of Tyr-291 is crucial for orienting HKV in the active site before the reaction.

Although the hydroxyl oxygen (O4) of both the S-HKV and R-HKV in Tyr291Phe forms stable H-bonds with two water molecules (Fig. 3 *E*), in Tyr291Ser it rapidly (within 0.15 ns) forms a direct H-bond (with a mean separation of ~1.8 Å between the HKV O4 hydroxyl hydrogen donor atom and the Asp-53 carboxylate oxygen acceptor atom) with Asp-53 after an initial separation of 6.2 Å. In both of these mutants, a combination of water and Asp-53 appears to take on the role of Tyr-291 in maintaining the orientation of HKV within the active site. The close proximity of Asp-53 to the substrate in the Tyr291Ser mutant suggests that it may be able to take on the role of proton shuttle in the absence of Tyr-291 if one is required in this reaction. This interaction could explain why BphI-BphJ did not lose total activity in the Tyr290Ser mutant.

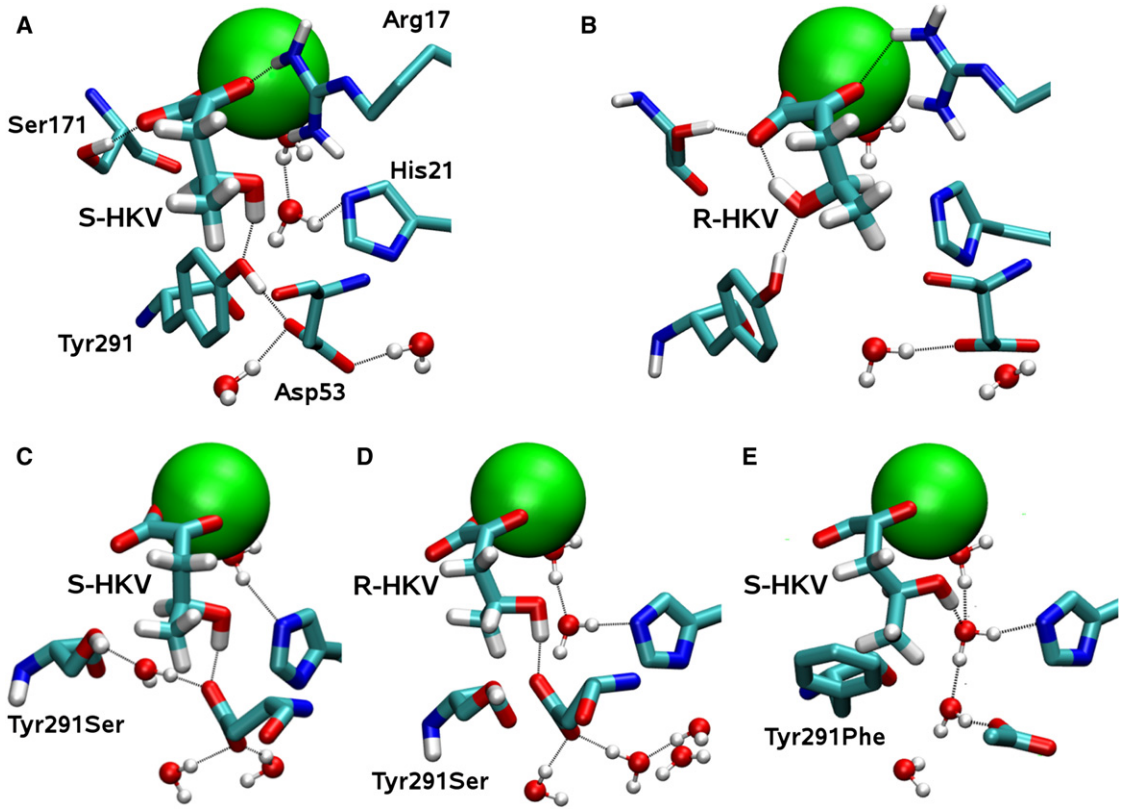

FIGURE 3 Stereoselectivity in WT and mutant DmpFG. Snapshots from MD simulations showing (*A*) S-HKV in WT DmpFG; (*B*) R-HKV in WT DmpFG, where HKV folds back on itself, forming an interaction between H4 and O3 and the methyl group is oriented toward His-21, avoiding a steric clash with Tyr-291; and (*C* and *D*) S and R-HKV, respectively, in the Tyr291Ser mutant. Note that Asp-53 changes orientation (relative to *A*, *B*, and *E*), forming a direct H-bond with HKV H4. (*E*) S-HKV in the Tyr291Phe mutant. Mn^{2+} is shown as the large sphere and important residues are labeled.

HT and Cys-132

Having found that AALD could easily enter the channel, we sought to determine whether it could move through the channel to the dehydrogenase active site. Before examining this directly, however, we first looked at the behavior of the other suggested control point, the HT, and the dynamics of the putative catalytic residue, Cys-132.

We analyzed the behavior of the three residues of the HT using the 200 ns equilibrium MD simulations. Although the system with NAD^+ has a slightly larger area between the residues of the HT than the system without NAD^+, the moving averages shown in Fig. 4, *D* and *E*, show that the behavior of the HT is essentially the same in the deprotonated systems regardless of the presence of NAD^+. This is interesting because Manjasetty et al. (2) suggested that it was the presence of NAD^+ that triggered the HT to change from a closed to an open state. Our results suggest that the protonation state of Cys-132 has a greater influence on the behavior of the HT. Fig. 4, *D* and *E*, clearly shows that regardless of the presence of NAD^+, when Cys-132 was protonated, the fluctuations of the HT were minimized and the area between the residues through which AALD must move to enter the channel was smaller. This implies that protonated Cys-132 stabilizes the HT in such a way that the AALD is less likely to enter the active site. This in turn implies that the AALD is most likely to enter the DmpF active site for dehydrogenation and acetylation when Cys-132 is deprotonated and ready to react. The fact that the area between the HT changes so dramatically shows how flexible the HT is, and that it does indeed move between a closed and an open state. However, it also raises the question: How does the protonation state of Cys-132 trigger this dramatic change in behavior? Although this question is currently unanswered, it is clear that the HT is a control point gating exit from the channel.

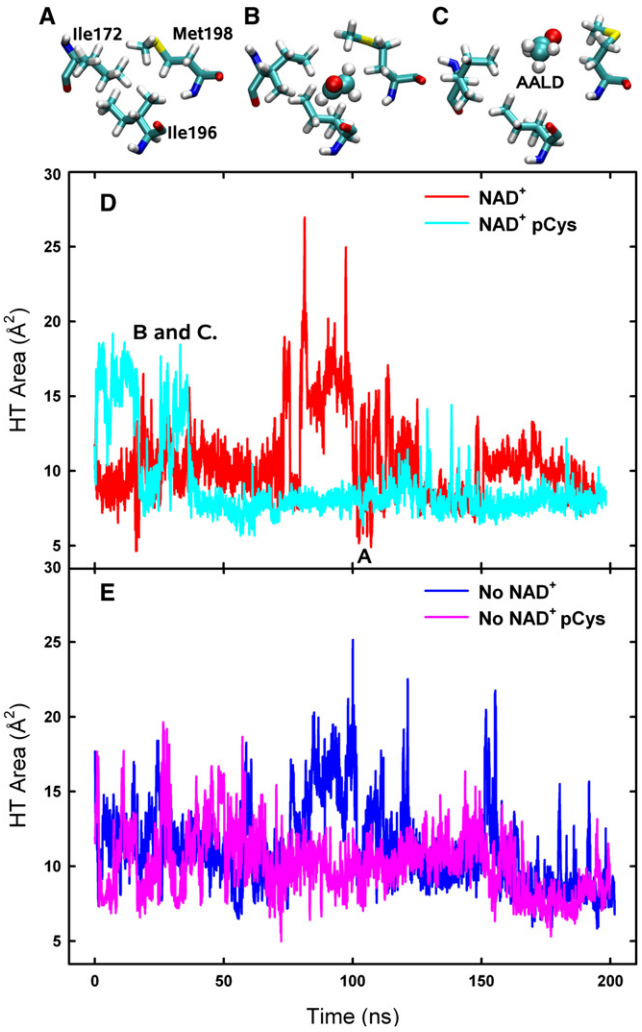

FIGURE 4 Behavior of the HT with time. (*A–C*) Snapshots of the HT at times indicated by A–C on graph *D* for the system with NAD^+ and protonated Cys-132. (*A*) HT in its closed state. (*B* and *C*) The minimum (6.3 $Å^2$) and maximum (22 $Å^2$) areas obtained with AALD in the HT. (*D* and *E*) A moving average of the area between the residues that form the HT through which AALD can pass, calculated throughout the 200 ns MD simulations for the systems with (*D*) and without (*E*) NAD^+, and with protonated (pCys) and deprotonated Cys-132.

In the system with NAD^+ and protonated Cys-132, the AALD spent a significant amount of time within the HT (~25–40 ns; Fig. 4 *D*). We used the steps where AALD was within the HT to investigate this process further and found that when the HT was occupied by AALD, the mean area between the HT was 14.8 $Å^2$. This relatively high average supports the finding that in both simulations with protonated Cys-132, where the average value was consistently lower than that observed for the deprotonated systems (Fig. 4), the AALD had less chance of entering and subsequently passing through the HT. The maximum area obtained with AALD in the HT, 22 $Å^2$, occurred when Met-198 swung back and away from the HT toward Cys-132, and Ile-196 rotated such that its bulky methyl groups oriented toward the exterior of the HT (Fig. 4 *C*). In contrast, the HT was most closed when Met-198 swung away from Cys-132 and oriented its methyl group toward Ile-172 and Ile-196 (Fig. 4 *A*). Although each of these residues had multiple conformations during these simulations, it appears that the motion of Met-198 is of paramount importance in the movement of the HT between an open and closed state. This is further confirmed by the region from 75 to 100 ns for the deprotonated systems with and without NAD^+ in Fig. 4, where the largest HT areas are observed. This occurs when Met-198 swings away from the HT; however, the area noted here is greater at points because the methyl group can orient itself completely out of the HT.

Cys-132 is the strictly conserved, putative catalytic nucleophile that is required for the dehydrogenase reaction in DmpF, as discussed by Manjasetty et al. (2). In the case of DmpF, Cys-132 was found to have several positions in the crystal structure that differed depending on the presence

and absence of NAD^+. Specifically, in the absence of NAD^+, Cys-132 was observed to form a close interaction with Asp-209 via a bridging water molecule. When NAD^+ was bound to the enzyme, Cys-132 adopted a position in which the thiolate group was oriented toward the nicotinamide ring of the cofactor. This led Manjasetty et al. (2) to propose a mechanism for this dehydrogenase in agreement with a mechanism proposed by Hempel et al. (30) for CoA-independent aldehyde dehydrogenases. This process requires Asp-209 to activate the water molecule to form a base, which in turn attacks Cys-132, removing the proton from the sulfhydryl group. This mechanism is thought to change the conformation of the thiol group, allowing it to nucleophilically attack the AALD. Although useful hypotheses can be drawn from the structural data, these data do not give us insight into the protonation states of the residues at the time these interactions were formed. Altering the protonation state of Cys-132 in the presence and absence of NAD^+ in a series of equilibrium MD simulations should allow the observation of some interesting structural changes in DmpFG over time.

We followed the behavior of Cys-132 in two protonation states in the presence and absence of NAD^+. Three main orientations were sampled by Cys-132 over this time, as described by the dihedral C-CA-CB-SG shown in Fig. 5 *A*. Orientation 1, between $-50°$ and $-100°$, toward Asp-209 is common to both systems and can be seen in Fig. 5, *C* and *D*. Orientation 2, between $-150°$ and $-200°$, is oriented toward the NAD^+ pyridine ring, as shown in Fig. 5 *E*, when NAD^+ is present. In the absence of NAD^+, the same two positions are visited along with orientation 3, between $50°$ and $100°$. This occurs because in the absence of NAD^+, Cys-132 occupies a cavity between Asn-290, Met-294, and Pro-166, and can change its position between these residues. This is contrary to Manjasetty et al. (2), who predicted that Cys-132 would have an additional position in the presence of NAD^+.

We also hypothesized that Asp-209 would play a role in the DmpF reaction by removing a proton from a water molecule, which would then base attack Cys-132. Although initially the Cys-132 proton and Asp-209 were >8 Å apart, we noted that throughout the simulations Cys-132 would orient itself toward Asp-209 (Fig. 5 *F*). For the system with NAD^+, this change occurred quickly and the interaction was maintained for >12 ns, initially with a single water molecule forming a bridge between the two residues (Fig. 5 *C*) and then with a network of waters (Fig. 5 *D*). The minimum distance between the Cys-132 proton and Asp-209 was 4.0 Å, supporting the possibility of protons moving between these residues via the bridging water. Positions C and D in Fig. 5 correspond to the stepwise motion of Cys-132 away from Asp-209 (Fig. 5 *F*) when this interaction is broken and Cys-132 ultimately reorients toward NAD^+. Although this interaction between Cys-132 and Asp-209 was also observed in the system without

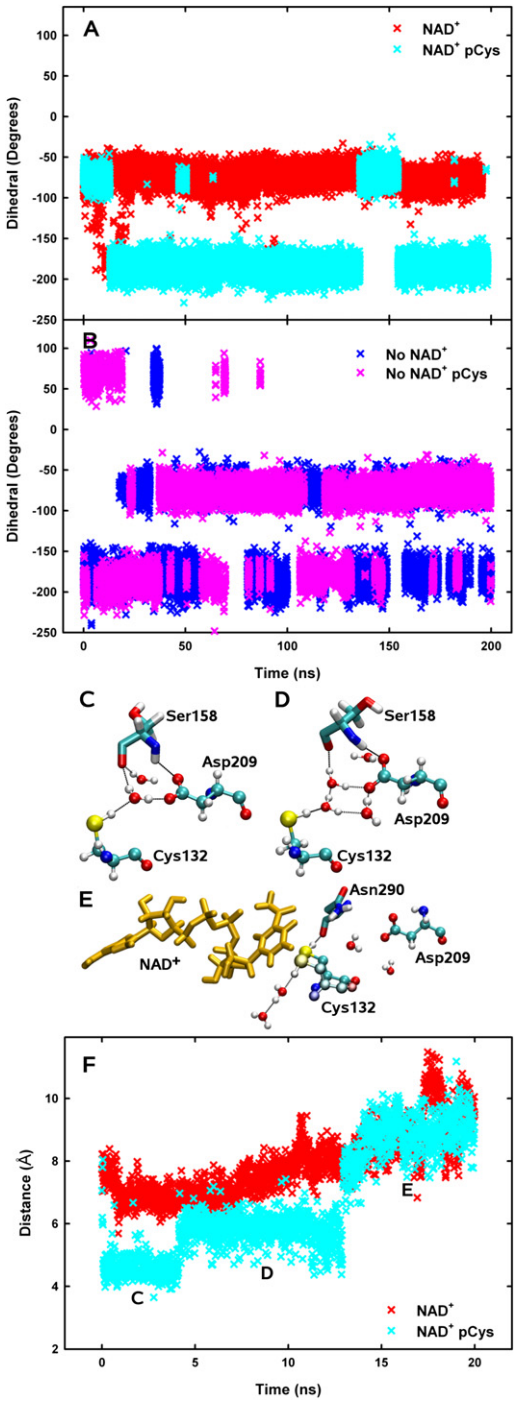

FIGURE 5 (*A* and *B*) Cys-132 dihedral (C-CA-CB-SG) calculated throughout the 200 ns MD simulations for the systems with (*A*) and without (*B*) NAD^+, and with protonated (pCys) and deprotonated Cys-132. (*C–E*) Orientations of Cys-132 in the presence of NAD^+. (*C*) Cys-132 is oriented toward Asp-209 with a single bridging water. (*D*) Cys-132 is still oriented toward Asp-209, but now three waters are present rather than one. (*E*) Cys-132 is oriented toward NAD^+. The sulfhydryl hydrogen of Cys-132 is free to rotate and forms two main interactions, the first with Asn-290 and the second with water. (*F*) The distance between the Cys-132 SH or S^- and Asp-209 for the NAD^+ systems with deprotonated and pCys, respectively, over 20 ns of the MD simulation. *C–E* represent the times captured in the three snapshots above.

NAD^+, the minimum distance was higher, with a value of 5.16 Å, and was maintained for <1 ns.

Escape from the channel

Throughout these simulations, we noted that the channel's structure was not fixed or uniform. The dynamic nature of the channel in DmpFG is not unexpected, because in a recent study of channeling in BphI-BphJ, Carere et al. (11) found that branched isobutyraldehyde was channeled with an efficiency similar to that of AALD. This suggests that constricted regions within the channel are able to move in such a way that they can accommodate larger substrates. Although this fluidity in the structure of the channel provides advantages in terms of channeling intermediates of different sizes, we also noted that over the course of the MD simulations, routes out of the channel opened up, allowing the AALD to escape. In addition to these transient gaps along the length of the channel, in the absence of NAD^+, a large cavity, open to the bulk media, is present in the dehydrogenase active site where NAD^+ would normally be positioned.

Channeling between multienzyme subunits is not always an efficient process. In practical terms, kinetic assays are often designed to ascertain the leakiness of the channel in question. For example, Baker et al. (9) found that in the presence of a large excess of exogenous propionaldehyde and limited substrate HKV, 95% of the CoA esters produced by BphI-BphJ were acetyl CoA. Similarly, when excess AALD was added exogenously with 4-hydroxy-2-oxohexanoate, 99% of the CoA esters formed were propionyl CoA. These results suggest that both the channel and the active site of BphJ are fairly impermeable to the entry of aldehydes from the bulk media. Carere et al. (11) recently found that the specific efficiency of channeling AALD was ~95%. In contrast, the specific efficiency of reverse channeling in BphI-BphJ was quantified as 84% (10). This indicates that there are possible escape routes for the aldehyde intermediates in the channel. Because DmpFG is similar to BphI-BphJ, one would expect it to share this trait. It would be difficult to observe where the AALD exits the channel in experiments; however, escape was observed during the MD simulations and the escape route can be located (Fig. S4).

In these simulations, AALD always left the protein in the vicinity of the dimerization domain between the DmpG and DmpF subunits. In three of the four systems, this occurred from the DmpG side of the channel in line with Leu-90 (at ~−3 Å in our definition of positions in the channel) as shown in Fig. S3 for both systems without NAD^+ (*dark blue and magenta lines*) and the system with NAD^+ and deprotonated Cys-132 (*red line*). This occurred as a continual path of water formed from the channel to the bulk media over the course of the simulation. In the fourth system, with NAD^+ and protonated Cys-132 (*cyan line*), AALD left near the HT at ~5 Å. Snapshots of the exit routes of AALD from the channel are shown in Fig. S4.

The fact that AALD can leave the channel in DmpFG does not mean that it will do so every time. To further investigate channeling within this enzyme, we examined the energetics of motion from the aldolase to the dehydrogenase active site. In the 200 ns equilibrium MD simulations, AALD only went through the HT in the system with NAD^+ and protonated Cys-132. This occurred within 25 ns, and after moving through the HT, AALD was able to move into the region of the DmpF active site. AALD was free to move back and forth through the HT, and it approached the NAD^+ three times over ~10 ns. Subsequently, AALD exited the HT and then left the protein 100 ns later, as shown in Fig. S3. This shows that it is indeed possible for AALD to travel through the channel from one active site to the other, and provides a possible timescale for this event. However, because it did not occur in each simulation, and the protonation state of Cys-132 was not suitable for the DmpF reaction to take place, further investigation of AALD transport is advisable.

Energetics of channeling

We have now shown that AALD can enter the channel in the presence and absence of NAD^+; therefore, the final aspect of this process to be determined is whether it is energetically feasible for AALD to move through the HT and into the dehydrogenase active site in both cases. The channel's nonuniformity combined with the long side chains of the hydrophobic amino acid residues that form the channel walls (e.g., Leu-90, Pro-91, Val-121, and Met141) makes the process of effectively sampling the entire region very time-consuming and computationally demanding. The large time requirement is further compounded by the fact that AALD is able to leave the channel prematurely. Although boundary walls can be applied within the framework of metadynamics if they are in the region of interest, this approach can alter the final free-energy values obtained. To overcome this issue, we obtained multiple free-energy profiles and averaged the results to allow sufficient sampling from one active site to the other.

In the presence of NAD^+, the free-energy change required for AALD to move from the aldolase to the dehydrogenase active site was −5.8 kcal/mol in a predominantly downhill process, as shown in Fig. 6. The largest barrier posed to the passage of AALD was 4.4 kcal/mol and can be assigned to bulky residues located around the dehydrogenase active site, including the residues of the HT and Phe-175 (Fig. S1). Because the channel is lined by a series of nonpolar residues, AALD diffuses freely without a preferred orientation, rather than forming specific interactions as was observed for channeling in the enzyme carbamoyl phosphate synthetase (17). In the absence of NAD^+, the free energy required for AALD to move from the aldolase to the dehydrogenase

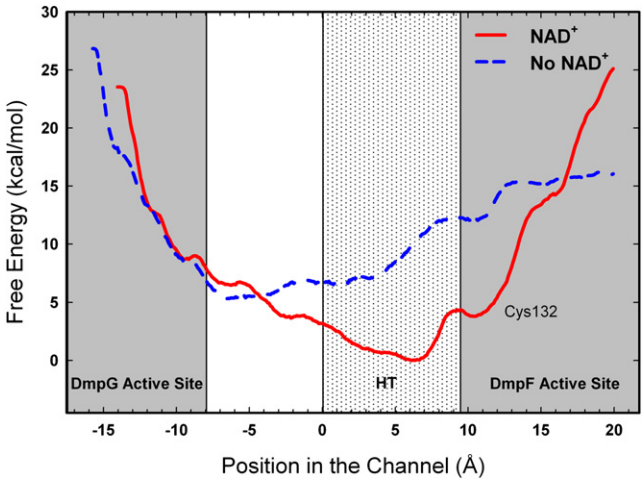

FIGURE 6 Free-energy profiles obtained for the systems with and without NAD^+. The gray-shaded areas show the regions in close proximity to the DmpG and DmpF active sites. The spotted region indicates where interactions occur between AALD and the three residues of the HT. In these simulations, AALD begins at ~−10 Å on this scale relative to the 0 Å point indicated.

active site changed significantly to +3.4 kcal/mol. The overall shape of the free-energy landscape and the total change in free energy suggest that the AALD is far less likely to reach the DmpF active site if NAD^+ is absent due to barriers near Leu-90, created by the bulky side chain impeding the passage of AALD, and the HT. This implies that the channeling of AALD from the aldolase to the dehydrogenase active site is energetically more feasible in the holo-enzyme form of DmpFG. The free-energy profile in the absence of NAD^+ seems to favor the transport of AALD in the reverse direction. This would allow AALD that is generated in the second active site from acetyl-CoA to be transported back through the channel to the aldolase active site with a change in free energy of −3.4 kcal/mol. This is not unexpected, because the reverse reaction was previously observed in BphI-BphJ (10). This drastic coenzyme-dependent change in the free-energy profiles supports the use of allosteric coupling between the subunits of DmpFG.

CONCLUSION

Understanding the mechanisms of substrate channeling within multienzyme systems is of paramount importance because this process occurs in so many key biochemical pathways (4,6,3). Although structural, mutation, and kinetic studies have highlighted important residues, many questions remain unanswered. Several computational studies have furthered our understanding of the dynamics of substrate channeling. For example, Brownian dynamics was applied to study the movement of intermediates along external electrostatic highways in the enzymes dihydrofolate reductase-thymidylate synthase (31) and in a fusion protein of malate dehydrogenase and citrate synthase (18). In both cases it was found that the substrate was prevented from entering the bulk media by its strong electrostatic interactions with the surface of the protein. In terms of channeling via buried molecular channels, both a free-energy MD study of the enzyme CPS (17) and a steered MD study of imidazole glycerol phosphate synthase (32) showed that the intermediates were channeled via the exchange of multiple H-bonds. In contrast to the above enzyme systems, in this study we found that AALD is channeled through DmpFG via simple diffusion. This means that AALD is free to move back and forth in the channel, protecting the reactive intermediate whichever way the reaction proceeds. However, if NAD^+ is bound to the enzyme, it is more energetically favorable for AALD to move from the DmpG to the DmpF active site.

Because no H-bonds are formed and broken during the transport of AALD, there are potential advantages in terms of the timescale of this event relative to the other channeling systems discussed above. At present, there is no definitive way to theoretically calculate the rate of transport through a buried molecular channel, because the substrate is moved in a predominantly one-dimensional process rather than a random walk (3). Recently, Huang et al. (3) suggested that the linear migration of proteins on DNA (another one-dimensional transport process) is analogous to the transport of intermediates through a molecular tunnel. Applying that reasoning to DmpFG yields a rate of ~ 34,000 s^{-1}, equivalent to a journey time of ~29.2 μs. However, our simulations show that an individual event can be as short as 25 ns, and the slope of the energy landscape can be expected to speed up the transport compared with Huang et al.'s calculation.

We also found that although Tyr-291 favors two main orientations, it does not act as a gate to control the movement of AALD into the channel. Instead, it is thought to play a role in orienting the substrate HKV within the DmpG active site before the reaction, and may serve as a proton shuttle. We found that the HT, another proposed gate, acts as a control point in the channeling process moving between an open and closed state. This movement was greatly minimized when Cys-132 was protonated, suggesting an allosteric interaction within the DmpF subunit coupling the readiness of the second active site to the transport of the intermediate. In addition, Cys-132 was found to occupy multiple positions, supporting the hypotheses of Manjasetty et al. (2). Finally, we have shown that the channeling of AALD from the DmpG to the DmpF active site in the enzyme DmpFG is energetically feasible in the presence of NAD^+.

SUPPORTING MATERIAL

Four figures showing the structure of the channel, the behavior of Tyr-291, and the escape routes from the channel are available at http://www.biophysj.org/biophysj/supplemental/S0006-3495(12)00111-7.

The authors gratefully acknowledge an award under the Merit Allocation Scheme on the National Computational Infrastructure National facility at the Australian National University, and computer time from iVEC.

REFERENCES

1. Srere, P. A. 1987. Complexes of sequential metabolic enzymes. *Annu. Rev. Biochem.* 56:89–124.
2. Manjasetty, B. A., J. Powlowski, and A. Vrielink. 2003. Crystal structure of a bifunctional aldolase-dehydrogenase: sequestering a reactive and volatile intermediate. *Proc. Natl. Acad. Sci. USA.* 100:6992–6997.
3. Huang, X., H. M. Holden, and F. M. Raushel. 2001. Channeling of substrates and intermediates in enzyme-catalyzed reactions. *Annu. Rev. Biochem.* 70:149–180.
4. Milani, M., A. Pesces, …, P. Ascenzi. 2003. Substrate channeling. *Biochem. Mol. Biol. Educ.* 31:228–233.
5. Miles, E. W., S. Rhee, and D. R. Davies. 1999. The molecular basis of substrate channeling. *J. Biol. Chem.* 274:12193–12196.
6. Weeks, A., L. Lund, and F. M. Raushel. 2006. Tunneling of intermediates in enzyme-catalyzed reactions. *Curr. Opin. Chem. Biol.* 10: 465–472.
7. Shingler, V., J. Powlowski, and U. Marklund. 1992. Nucleotide sequence and functional analysis of the complete phenol/3,4-dimethylphenol catabolic pathway of *Pseudomonas* sp. strain CF600. *J. Bacteriol.* 174:711–724.
8. Agarry, S., and A. Durojaiye. 2008. Microbial degradation of phenols: a review. *Int. J. Environ. Pollut.* 32:12–28.
9. Baker, P., D. Pan, …, S. Y. K. Seah. 2009. Characterization of an aldolase-dehydrogenase complex that exhibits substrate channelling in the polychlorinated biphenyls degradation pathway. *Biochemistry.* 48:6551–6558.
10. Wang, W., P. Baker, and S. Y. K. Seah. 2010. Comparison of two metal-dependent pyruvate aldolases related by convergent evolution: substrate specificity, kinetic mechanism and substrate channelling. *Biochemistry.* 49:3774–3782.
11. Carere, J., P. Baker, and S. Y. K. Seah. 2011. Investigating the molecular determinants for substrate channelling in BphI-BphJ, an aldolase-dehydrogenase complex from the polychlorinated biphenyls degradation pathway. *Biochemistry.* 50:8407–8416.
12. Baker, P., J. Carere, and S. Y. K. Seah. 2011. Probing the molecular basis of substrate specificity, stereospecificity, and catalysis in the class II pyruvate aldolase, BphI. *Biochemistry.* 50:3559–3569.
13. Powlowski, J., L. Sahlman, and V. Shingler. 1993. Purification and properties of the physically associated meta-cleavage pathway enzymes 4-hydroxy-2-ketovalerate aldolase and aldehyde dehydrogenase (acylating) from *Pseudomonas sp*. strain CF600. *J. Bacteriol.* 175:377–385.
14. Doukov, T. I., T. M. Iverson, …, C. L. Drennan. 2002. A Ni-Fe-Cu center in a bifunctional carbon monoxide dehydrogenase/acetyl-CoA synthase. *Science.* 298:567–572.
15. Darnault, C., A. Volbeda, …, J. C. Fontecilla-Camps. 2003. Ni-Zn-[Fe_4-S_4] and Ni-Ni-[Fe_4-S_4] clusters in closed and open subunits of acetyl-CoA synthase/carbon monoxide dehydrogenase. *Nat. Struct. Biol.* 10:271–279.
16. Krahn, J. M., J. H. Kim, …, J. L. Smith. 1997. Coupled formation of an amidotransferase interdomain ammonia channel and a phosphoribosyl transferase active site. *Biochemistry.* 26:11061–11068.
17. Fan, Y., L. Yang, …, Y. Gao. 2008. Mechanism for the transport of ammonia within carbomoyl phosphate synthetase determined by molecular dynamic simulations. *Biochemistry.* 47:2935–2944.
18. Elcock, A. H., and J. A. McCammon. 1996. Evidence for electrostatic channeling in a fusion protein of malate dehydrogenase and citrate synthase. *Biochemistry.* 35:12652–12658.
19. Essmann, U., L. Perera, and M. L. Berkowitz. 1995. A smooth particle mesh Ewald method. *J. Chem. Phys.* 103:8577–8593.
20. MacKerell, Jr., A. D., D. Bashford, …, M. Karplus. 1998. All-atom empirical potential for molecular modelling and dynamics studies of proteins. *J. Phys. Chem. B.* 102:3586–3616.
21. MacKerell, Jr., A. D. 2001. Atomistic models and force fields. *In* Computational Biochemistry and Biophysics. O. M. Becker, A. D. MacKerell, Jr., B. Roux, and M. Watanabe, editors.; Marcel Dekker, New York. 7–38.
22. Singh, U., and P. Kollman. 1984. An approach to computing the electrostatic charges for molecules. *J. Comput. Chem.* 5:129–145.
23. Besler, B., K. Merz, Jr., and P. Kollman. 1990. Computer modeling of the interactions of complex molecules. *J. Comput. Chem.* 11:431–439.
24. Batsanov, S. 2001. Van der Waals radii of elements. *Inorg. Mater.* 37:1031–1046.
25. Frisch, M. J., G. W. Trucks, …, J. A. Pople. 2004. Gaussian 03, revision C.02. Gaussian, Inc., Wallingford, CT.
26. Phillips, J. C., R. Braun, …, K. Schulten. 2005. Scalable molecular dynamics with NAMD. *J. Comput. Chem.* 26:1781–1802.
27. Humphrey, W., A. Dalke, and K. Schulten. 1996. VMD: visual molecular dynamics. *J. Mol. Graph.* 14:33–38, 27–28.
28. Laio, A., and F. L. Gervasio. 2008. Metadynamics: a method to simulate rare events and reconstruct the free energy in biophysics, chemistry and material science. *Rep. Prog. Phys.* 71:126601–126622.
29. Laio, A., and M. Parrinello. 2002. Escaping free-energy minima. *Proc. Natl. Acad. Sci. USA.* 99:12562–12566.
30. Hempel, J., J. Perozich, …, B. C. Wang. 1999. Aldehyde dehydrogenase catalytic mechanism. A proposal. *Adv. Exp. Med. Biol.* 463:53–59.
31. Elcock, A. H., M. J. Potter, …, J. A. McCammon. 1996. Electrostatic channeling in the bifunctional enzyme dihydrofolate reductase-thymidylate synthase. *J. Mol. Biol.* 262:370–374.
32. Amaro, R., and Z. Luthey-Schulten. 2004. Molecular dynamics simulations of substrate channelling through an α-β barrel protein. *Chem. Phys.* 307:147–155.